Photothermal studies of single molecules and gold nanoparticles : vapor nanobubbles and conjugated polymers

Hou, L.

1

Introduction

In this thesis, we report properties and dynamics of vapor nanobubbles in liquid (first-order phase transition) around a laser-heated single gold nanoparticle (plasmon-mediated vapor nanobubbles), and we measure the absorption and emission of single conjugated polymer molecules poly[2- methoxy- 5 -(2-ethylhexyloxy)-1,4 - phenylenevinylene] (MEH-PPV) using near-critical xenon (second-order phase transition) to enhance the absorption signal. In this chapter, we will give an overview and motivation of our research and outline the contents of this thesis.

1.1. First-order and second-order phase transitions

In our daily life, phase transitions of water are observed everywhere: liquid water boils into vapor in the saucepan; frost forms at the surface of a window in a cold winter. If you look at the phase diagram of water as shown in Fig.1.1, phase transitions take place at different temperatures and pressures between adjacent regions in the diagram. The curve between liquid and vapor in the diagram is the saturation curve where liquid and vapor phases coexist. Normal boiling of water happens when the liquid is heated up at ambient pressure and crosses the saturation curve along the horizontal line at $p = 1$bar. We can also find the critical point of water above which liquid and vapor phases are not distinguishable, and a single phase supercritical water forms. People use "thermodynamic state functions" to describe the thermodynamics of phase transitions. For instance, the internal energy of a system U is a state function $U(S,V)$ where S is the entropy, V is the volume. Other common thermodynamic state functions include the enthalpy $H(S,P) = U + pV$, the Gibbs potential or Gibbs

free energy $G(T,P) = H - TS$ (T is the temperature), and the Helmholtz potential or Helmholtz free energy $F(T,V) = U - TS$. In the transformation of two phases such as from liquid to vapor, there often is finite discontinuity in the first derivative of the Gibbs potential $G(T,P)$ ($\partial G/\partial T = -S, \partial G/\partial P = V$) [1]. This process is called a first-order phase transition. Obviously the first-order transition is accompanied with a discontinuity in entropy and exchange of latent heat. Correspondingly, the second-order phase transition refers to the continuity in the first derivative of the Gibbs potential and discontinuity in the second-order derivative with respect to an external variable such as temperature or pressure. Above the critical point, one can convert liquid to vapor or vice versa continuously without crossing the coexistence curve. An important feature of a second-order phase transition is that response functions such as the heat capacity and the compressibility diverge at the critical point. This effect causes large fluctuations in the density in response to a little change of temperature and pressure, and can be useful in some circumstances. We will discuss the first-order transition of water at nanometer scale, which is the vapor nanobubbles' formation around a nano-size absorber such as a gold nanoparticle in Chapters 2, 3 and 4. We utilize the second-order transition of xenon to enhance the photothermal contrast (absorption signal) of single conjugated polymer molecules, which will be discussed in Chapters 5 and 6.

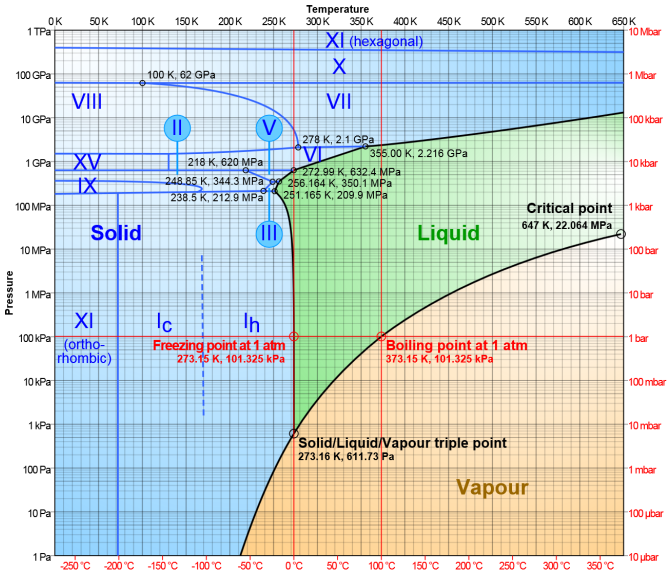

Figure 1.1: Pressure-temperature phase diagram of water [2]. The Roman numerals indicate various ice phases.

1.2. Vapor nanobubbles and applications

Properties of bubbles in a liquid with different sizes, from centimeters to nanometers, and different contents (dissolved gas or vapor) have been extensively studied over the past years [3–5], and research in this field remains active nowadays. This is not only because bubbles show complex physical behaviors (such as sonoluminescence and shock-wave release), but they also are potentially useful or detrimental for various applications (for cleaning and ship-propeller erosion through cavitation). In particular, we are interested in the vapor nanobubbles that arise upon crossing the saturation line of liquid-vapor coexistence and with a size of typically a few tens to hundreds of nanometers. Due to the confinement of temperature and pressure at nanometer scales, high compressibility and large optical scattering cross section, vapor nanobubbles are believed to be useful in many applications such as photothermal therapy [6], drug delivery [7], enhancing catalytic reactions and enhancing coupling between optical and acoustic waves [8]. For example, Lukianova-Hleb *et al.* have showed that by generating small vapor nanobubbles specifically in malaria parasites using laser pulses, one can diagnose and get rid of infected blood red cells in a patient's body without any labeling and invasive treatment [9]. Goy *et al.* have shown that generation of vapor nanobubbles improves the resolution of photoacoustic imaging by a factor of two [10]. Adleman *et al.* demonstrated that vapor bubbles generated by plasmonic heating facilitate catalytic reactions [11].

Since vapor nanobubbles are so useful in many circumstances, the main motivation of this thesis is to study the physical properties and dynamics of such tiny vapor bubbles in order to gain a better understanding of their nature, as well as to seek a way to control and make use of them for applications. Because of their small size, vapor nanobubbles need to overcome a large Laplace pressure in order to nucleate and grow. Thus a bubble requires more heat and energy to form at nanometer scale, and temperature and pressure will shift to much higher values than at ambient conditions. Classical nucleation theory and experimental observation point out that when the liquid is heated up to a high enough temperature, boiling and phase transition show explosive nature [12]. The small nanometer size also means that the time scale for transient vapor nanobubbles becomes very short [13]. All these factors add up and make the study of vapor nanobubbles quite challenging. In this thesis, we aim for the answer to a number of key questions regarding the physical properties of vapor nanobubbles such as temperature and pressure upon bubble formation; whether vapor nanobubbles are in equilibrium with the surrounding liquid or highly dynamical; how vapor nanobubbles interact with local surroundings such as nearby interfaces and how vapor nanobubbles behave during for-

mation and collapse on different time scales. Since a gold nanoparticle is an efficient local-heat absorber under optical excitation, we constrain our discussion to the plasmon-mediated steam nanobubbles that form in a liquid around an optically heated single gold nanoparticle. The advantage of an all-optical detection is its speed, sensitivity and non-invasive character.

1.3. Theoretical models to describe vapor bubble physics

In order to gain a better understanding of the physics of vapor nanobubbles and to explain existing results, a number of models and simulation methods have been proposed and applied to bubble studies [3]. Here we briefly introduce some of the common modeling methods used in the theoretical study of bubble dynamics, covering both continuum approaches and numerical simulations.

1.3.1. Rayleigh-Plesset equation

In 1917, Rayleigh derived an equation to describe the problem of cavitation and bubble dynamics with spherical geometry in an infinite liquid [14]. In his model, he considered the collapse of a void cavity in an infinite liquid, neglecting the surface tension and liquid viscosity presumably because only large bubbles were considered at that time. He also assumed that the liquid is incompressible and pressure far away from the bubble keeps constant. The equation is written as:

$$R(t)\frac{d^2R(t)}{dt^2}+\frac{3}{2}\left[\frac{dR(t)}{dt}\right]^2=\frac{1}{\rho}\{P[R(t)]-P_\infty\} \tag{1.1}$$

where $R(t)$ is the bubble radius; the pressure in the bubble is $P(R)$; the pressure at the place of infinity in the liquid is P_∞, and ρ is the liquid density. Later Plesset modified Rayleigh's equation, taking into account the surface tension and liquid viscosity, and rewrote the Rayleigh equation and got the well-known "Rayleigh-Plesset" equation, which is widely used in cavitation modeling and bubble dynamics simulations [15]. It is written as:

$$R(t)\frac{d^2R(t)}{dt^2}+\frac{3}{2}\left[\frac{dR(t)}{dt}\right]^2=\frac{1}{\rho}\left\{P(t)-P_\infty(t)-\frac{2\gamma}{R(t)}-\frac{4\mu}{R(t)}\frac{dR(t)}{dt}\right\} \tag{1.2}$$

The terms on the right-hand side of the equation 1.2 are the bubble internal pressure, the pressure at infinity, the Laplace pressure (γ is the surface tension) and μ is the liquid viscosity, respectively. In this equation, the liquid is still assumed to be incompressible. The Rayleigh-Plesset equation can be derived from a continuum theory [3].

Since then, the Rayleigh-Plesset equation has been applied to many problems regarding the temporal evolution of bubble size and has given satisfactory results on a number of bubble phenomena such as bubble bouncing after collapse [16], the emission of acoustic waves after a bubble's collapse, bubble oscillation in the acoustic field [4], and the natural oscillation frequency of a gas bubble, also known as the "Minnaert" frequency [17]. When modeling the cavitation and vapor bubble dynamics, compressibility of the liquid, mass and heat transfers, momentum and energy conservation should be considered as well. Nevertheless, modeling with the Rayleigh-Plesset equation seems quite successful in explaining many experimental data [18].

1.3.2. Gilmore equation

Another modeling approach to bubble dynamics was introduced by Gilmore in 1952, based on the hypothesis of Kirkwood and Bethe [19]. In his expression, Gilmore includes the effects of surface tension, viscosity, and the second power of the ratio of bubble wall velocity to the sound velocity (he called higher order compressibility terms), because compressibility of the liquid becomes significant and non-negligible when bubble wall velocity gets close to the speed of sound during bubble collapse. The equation is written as follows:

$$R\frac{d^2R}{dt^2}\left(1-\frac{1}{C}\frac{dR}{dt}\right)+\frac{3}{2}\left(\frac{dR}{dt}\right)^2\left(1-\frac{1}{3C}\frac{dR}{dt}\right)=H\left(1+\frac{1}{C}\frac{dR}{dt}\right)+\frac{R}{C}\left(1-\frac{1}{C}\frac{dR}{dt}\right)\frac{dH}{dt} \tag{1.3}$$

where H and C are the specific enthalpy of the surrounding liquid and the sound velocity at the bubble-liquid interface. Normally an equation of state is also needed to relate H and C with the pressure at the bubble wall, which is essentially a function of bubble radius and time. The Gilmore equation can be used for bubble dynamic modeling, but often it is used in the description of phenomena related to under-water explosions and in the calculation of radiated acoustic energy [20]. Note that the modeling of acoustic radiation is not restricted to the Gilmore equation, and it can be incorporated into Rayleigh-Plesset equation as well [21].

1.3.3. Molecular dynamics simulation

With the increase of computing power, molecular dynamics (MD) simulation can be exploited to simulate the bubble behavior and to predict real measurements. The idea behind MD is straightforward: given a number of interacting molecules, their interatomic potentials and certain boundary conditions, the trajectories of molecules can be solved numerically using the classical Newton

law of motion. The overall response can be obtained by integrating all equations [22]. For example, MD simulation has been applied to bubbles in a confined nano-channel to explain the nanobubble nucleation process [23]. MD simulation has its own limitations. It heavily depends on the parameters set in the simulation, and the number of molecules cannot be arbitrarily set; in some potential models, dielectric properties of the environment are not properly considered [22].

1.4. Methods to generate and probe vapor nanobubbles

Over the past decades, many techniques and methods have been applied to the study of vapor nanobubbles. In the following, we will briefly introduce some common methods used in research for generating and detecting vapor bubbles in liquid. In general, the methods used to form bubbles in liquid include: 1) applying negative pressure to the liquid at constant temperature with acoustic waves; 2) electric discharging in the liquid; 3) focusing a laser beam into the liquid with or without absorbing ions or nanoparticles. Correspondingly, the detection of bubbles can be achieved by: 1) monitoring the response of acoustic transducers; 2) monitoring a conductance change across a device; 3) monitoring wide-field optical image or scattering of bubbles. Different combinations of these methods are also widely used in the vapor bubble research. Other techniques such as AFM, in principle, can be used to study bubble's size and morphology. But the time resolution of AFM seems too slow to follow the dynamics of transient vapor bubbles, so we will not discuss it any further. For simplicity, we classify all these methods into three types: acoustical, electrical and optical, as shown in the schemes of Fig.1.2.

Acoustical: vapor bubbles can form in a liquid when the liquid pressure falls below the vapor (saturation) pressure. This process is normally called "cavitation" in the literature [3], even though there is no fundamental physical difference when it is compared with "boiling" where the temperature of liquid is raised above the (saturated) vapor temperature. When the liquid is subjected to a negative acoustic pressure which stretches liquid molecules apart, a nucleation can form at a "weak" site and develop into a bubble. Acoustic cavitation and associated bubbles are widely used in biomedical applications such as drug delivery and ultrasound imaging [24]. A common feature accompanying bubble's formation and collapse is the release of acoustic waves. The pressure waves released by bubbles can be picked up by some acoustic transducers and further amplified to produce a typical bubble signal [25]. The drawback of acoustic detection is the slow response of acoustic detectors. Most acoustic transducers have a resonant frequency around 10 MHz where sensitivity is

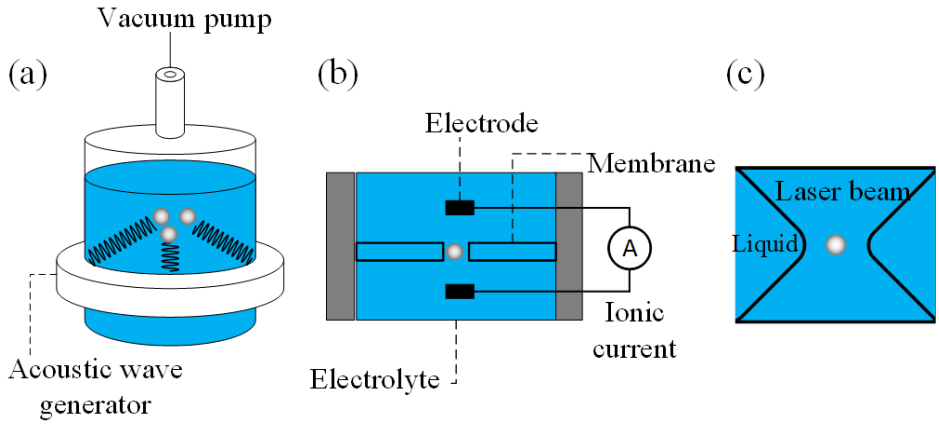

Figure 1.2: Schemes of methods used in the vapor bubble studies. a) acoustical; b) electrical; c) optical methods.

optimal. But the transient time of vapor nanobubbles can be as short as a few nanoseconds [26]. Thus, acoustic detectors are not fast enough to follow the dynamics of vapor nanobubbles.

Electrical: another common method of generating vapor bubbles in a liquid is to discharge a capacitance into a circuit containing two electrodes close to each other in an electrolyte. Vapor bubbles can form at a point of low conductance because of the high Joule heating of the electrolyte when a high current pulse is applied to the electrodes [27]. Nanostructures such as nanopores made of silicon nitride can be used to further confine Joule heat in a small volume [28]. This method can be easily implemented in the lab and does not require expensive optics and lasers of the optical method. The main challenge of this method is the difficulty of putting electrodes at the desired sites. Detection of vapor bubbles can be achieved by monitoring the conductance of the electrolyte in the pore in real time with high time resolution, up to ns [28].

Optical: optical generation of nanobubbles in liquid can be done simply by focusing a laser beam into the solution. Depending on the delivered optical influence and physical mechanism, nanobubble formation can be classified into two types [29]: thermally induced vapor bubbles (the liquid is heated up to a temperature above the boiling temperature) and direct break-down of the liquid (liquid molecules are ionized and generate a hot plasma, which expands to form a bubble). Various nanoparticles, such as metallic nanoparticles [30–32], quantum dots [33, 34], core-shell hybrid nanostructures [35], and ions dissolved in the liquid [36] can be exploited to enhance the absorption of liquid at a specific wavelength and the heating efficiency. Pulsed laser sources give

rise to a high confinement of heat around the excited volume, whereas a continuous laser leads to a more extended steady-state temperature profile in the liquid [37]. In the latter situation, liquid superheating and explosive boiling are often involved [36].

Detection of optically generated vapor bubbles can be achieved by wide-field optical imaging [25] with a fast camera. For vapor nanobubbles, the size is beyond the optical diffraction limit. But we can study the vapor nanobubbles by looking at the scattering intensity of a probe laser beam with low intensity [25, 32], or by total internal reflection microscopy (TIRF) [38], or by looking at the shifts of the surface plasmon resonance (SPR) of gold nanoparticles if gold nanoparticles are used as local heat sources to form vapor bubbles, because the SPR is sensitive to the change in the local refractive index [39]. X-ray scattering can also be used to monitor the liquid-vapor transition and bubble dynamics because X-ray scattering is sensitive to changes in structure and interactions of molecules in matter [26].

In our research, we propose to generate and study vapor nanobubbles all optically with the high spatial resolution of photothermal microscopy and the high temporal resolution of pump-probe microscopy. We illuminate a single gold nanoparticle in a liquid with a wavelength in resonance with the absorption of the particle. Dynamics of vapor nanobubbles are monitored through the intensity change of a second beam with a different wavelength and relatively low power. The advantage of single particle measurements is that averaging is excluded and vapor nanobubbles can be studied under various conditions with good reproducibility. The advantages of an all-optical study are its fast response, high spatial and temporal sensitivity and the low invasiveness.

1.4.1. Photothermal microscopy

Photothermal microscopy is an indirect method for probing the non-radiative energy dissipation of an object under excitation [40]. Normally two continuous laser beams are involved in such an experiment. The heating beam is intensity-modulated at high frequency, and used to heat up the object and create a temperature and refractive index profile in its nearby medium [41]. The probe beam, which is spatially overlapped with the heating beam, is scattered by the local index gradient and interferes with a reference field, such as a reflection of the incident probe beam by a nearby interface or the transmitted probe beam. The interfering signal is then picked up by a photodiode, and the small changes in probe intensity are isolated by demodulating the signal with a lock-in amplifier. The photothermal signal is proportional to the heating and probe powers, the absorption cross section of the small object, and the thermal

properties of the transducing medium. It can be written as [42]:

$$S \approx \frac{1}{\pi\omega_0} n \left.\frac{\partial n}{\partial T}\right|_p \frac{1}{C_p \lambda^2 \Omega} \frac{\sigma_{abs}}{A} P_{heat} P_{probe} \Delta t \tag{1.4}$$

From the above equation, we can see a number of ways that can further improve the photothermal signal [42]. For example by increasing both heating and probe powers, by matching the index of sample and substrate to reduce the laser noise, by integrating for longer times, by using a transducing medium with good thermal properties, and by putting an isolating layer to further confine the heat around the sample. It has been shown that photothermal microscopy has a sensitivity capable of probing 1.4 nm gold nanoparticles [43, 44] and single organic molecules [45]. The detected temperature change can be as small as 80 mK [42].

1.4.2. Time-resolved pump-probe spectroscopy

Time-resolved pump-probe spectroscopy exploits two synchronized short pulses with different wavelengths. The pump pulse is used as a trigger to excite the sample out of its equilibrium state; then the transient relaxation of excited species such as electrons is monitored with the probe pulse as a function of time through changes in the absorbance or transmittance of the sample. The time interval Δt between pump and probe pulses is controlled by varying the optical delay between these pulses with a linear mechanical stage. Then the "snapshots" and dynamics of excited species are recorded as a function of time delay. In the pump-probe spectroscopy, the time resolution is limited by the pulse width, provided no time jitter takes place between excitation and relaxation. Because the low signal to noise ratio in single-shot measurements with the pump-probe method, accumulation of many pulsed events is necessary, so that jitter leads to a loss of time resolution. Modulation of pump intensity at higher frequency and picking up of small variations in the probe intensity with a lock-in amplifier will remove the slow-varying backgrounds and thus significantly increase the signal to noise ratio and sensitivity of experiments. This technique has been widely used in studies such as electron-phonon coupling in metallic nanoparticles [46].

1.4.3. Optical contrast

Now we discuss the optical signals measured in photothermal microscopy and pump-probe spectroscopy. In both schemes, the total intensity detected by the

photodetector is given by the following equation if the heating beam is completely rejected from the detection [47]:

$$I = \left| E_{ref} + E_{sca} \right|^2 . \tag{1.5}$$

We write the complex reference field E_{ref} and the scattered field E_{sca} as:

$$E_{ref} = rE_0, \tag{1.6}$$

$$E_{sca} = sE_0 e^{i\varphi}, \tag{1.7}$$

where r, s are real quantities; E_0 is the complex incident electric field; φ is the phase difference between the reference field and the scattered field. Substituting Eq.1.6 and Eq.1.7 into Eq.1.5, we get the total intensity detected by the detector:

$$I = |E_0|^2 (r^2 + 2|r||s| cos\varphi + s^2). \tag{1.8}$$

For the small nano-objects considered here, the last term in Eq.1.8 (intensity scattered by the object) is much weaker than the strong reference intensity, and can be safely neglected. The first term is just a constant bright "background" and is removed by the lock-in detection. Then the contrast of detected signal mainly arises from the cross term of interference [48]. From this equation, we can see that the scattered field should be coherent with the reference field, and the spatial modes should be largely overlapped, otherwise the cross term will average to zero. The reference field can be implemented in different ways. For example, it can be the probe beam reflected by a nearby interface, the transmitted probe beam passing through the particle in the forward direction [49], an auxiliary beam in a differential interference contrast microscope (DIC) [44], in a Michelson interferometer [50], or in a common-path polarization interferometer [51]. If we assume that the total noise is shot-noise limited and proportional to the square root of the total number of photons on the detector, which is essentially the square root of the probe intensity, $\sqrt{r^2 |E_0|^2}$, the signal to noise ratio (SNR) becomes:

$$SNR = \frac{2|E_0|^2 |r||s| cos\varphi}{\sqrt{r^2 |E_0|^2}} = 2Re(E_{sca}), \tag{1.9}$$

which is actually independent of the reference field, as long as this field remains much stronger than the scattered field. This implies that the strength of the reference field can be arbitrarily tuned according to specific experimental conditions without losing signal to noise ratio.

1.5. Second-order phase transition and supercritical fluid

As mentioned at the beginning of this chapter, a second-order phase transition occurs at the critical point and a discontinuity in the second derivative of Gibbs' free energy is found. The phase transition between liquid and vapor phases takes place smoothly/continuously without crossing the saturation curve above the critical point. A supercritical fluid is a substance at a temperature and pressure above the critical point, where liquid and vapor phases cannot be distinguished anymore. At the critical point, the correlation length (which defines the characteristic distance where microscopic variables such as density start to differ from their initial values) and the time scale for molecular reorganization become infinite. Another interesting property of a critical fluid is that the singular behavior in the vicinity of the critical point is only characterized by a set of "critical exponents", regardless of the chemical components [52]. Close to the critical point, a supercritical fluid exhibits large fluctuations in quantities such as the density in response to small changes in temperature and pressure, thus making many properties of supercritical fluids finely tunable. For example, carbon dioxide is commonly used in industry as a supercritical fluid to extract, dissolve, and decompose substances [53].

1.6. Gold nanoparticle as a nanoabsorber

In order to increase the absorbing efficiency of the liquid for incident light and create localized vapor nanobubbles, we use gold nanoparticles (mainly spheres) in this thesis as the absorbing agent in liquid. The optical properties of gold nanoparticles have been extensively studied for many years [54]. Due to their superior photo-stability, large extinction cross section compared with organic molecules and biocompatibility, gold nanoparticles are used in numerous applications in many disciplines [55–59]. The optical properties of gold nanoparticles are related to the localized surface plasmon resonance (SPR), which is the collective oscillation motion of electrons in the conduction band of gold driven by an external electromagnetic field. The SPR often manifests itself by a resonance peak in the extinction (sum of absorption and scattering) spectrum. The resonance position depends on the size and shape of gold nanoparticles and on the refractive index of the surrounding medium. In the current study, gold nanoparticles are chosen as efficient light absorbers and localized heating sources because of the resonant absorption in the visible range, high thermal conductivity, very high bulk melting point and fast heating process within gold upon optical excitation. Phase transitions such as vapor bubble formation around gold nanoparticle can be further "amplified" by the shift of the SPR

in response to a refractive index change. Apart from that, gold nanoparticles can be anchored on the specific site of targets by surface functionalization. All these factors make gold nanoparticles excellent agents for the study of vapor nanobubbles.

1.7. Conjugated polymers

Conjugated polymers are one type of organic molecules consisting of many alternating double and single carbon-carbon bonds. Just as in a semiconductor, photon absorption or emission are associated to the transition of a delocalized π electron between the highest occupied and the lowest unoccupied molecular orbitals. Therefore, the optoelectronic properties of conjugated polymers resemble those of semiconducting materials. Conjugated polymers are widely used in organic light-emitting devices [60], thin-film transistors, and solar energy harvesting devices [61]. The optical properties of conjugated polymers strongly depend on their conformation and microscopic structure, which have been intensively studied with single-molecule fluorescence microscopy [62, 63]. Many factors influence the properties of conjugated polymers, including the distribution of molecular weights, the polarity of solvents used in the sample preparation, the sample annealing conditions, the embedding matrix and the spin-coating parameters, leading to very complex behavior. A direct measurement of the conformation of a single conjugated molecule seems challenging, if not impossible. However, a measurement of the heat dissipated by a molecule upon excitation can determine the number and orientation of absorbing monomer units, and therefore provide indirect information about the polymer's conformation. This will help us to evaluate the quantum yield of single conjugated molecules, thus to shed light on the conjugated polymers used in devices and applications.

1.8. Outline of this thesis

To facilitate the reading of this thesis, we list the main contents of each chapter:

Chapter 2: We provide a simple model for the thermo-dynamical analysis of a vapor nanobubble assuming the vapor nanobubble is in equilibrium with the surrounding liquid. We calculated the minimal temperature as well as the pressure for different sizes of vapor nanobubbles. We also estimated the optical power required to deliver into the system in order to form a vapor bubble around a continuous laser-heated gold nanosphere, and the optical signal change due to the presence of a vapor nanobubble. The information obtained

from this model paves the way for our experimental study.

Chapter 3: We experimentally investigated the dynamics of vapor nanobubbles in liquids around a continuous laser-heated gold nanosphere. A number of interesting phenomena were observed in our measurements, such as the instability of the nanobubble under constant heating, and the explosive and echo-triggered formations of nanobubbles. We characterized the behavior of nanobubbles and estimated the temperature, pressure and size of nanobubbles based on the optical signal.

Chapter 4: Combining time-resolved pump-probe spectroscopy and CW heating, we probed vapor nanobubbles around a single gold nanosphere with pico-second time resolution. We revealed the nanobubble evolution in the first nano-second after femto-second optical pulse excitation/triggering.

Chapter 5: We demonstrated a way to further enhance the photothermal contrast of weak absorbing nano-objects. We use xenon under supercritical phase to maximize dn/dT so that we can use much less power in order to get a good photothermal signal, compared with a normal liquid case. We characterize the enhancement factor, the dependency on modulation frequency, and compare the data with literature and with a common liquid, glycerol.

Chapter 6: We applied the enhanced photothermal technique to the simultaneous measurements of the absorption and emission of single conjugated MEH-PPV polymer molecules. We get useful information such as monomer numbers in a conjugated molecule and the apparent quantum yield of single polymer molecules.